3D Characterization of Electrical Tree Structures

Roger Schurch[1], Jorge Ardila-Rey[2], Johny Montana[1] and **Alejandro Angulo[1]**
Universidad Técnica Federico Santa María
Departamento de Ingeniería Eléctrica
[1] Valparaíso / [2] Santiago, Chile

Simon M. Rowland and **Ibrahim Iddrissu**
The University of Manchester
School of Electrical and Electronic Engineering
Manchester, M13 9PL, United Kingdom

Robert S. Bradley
Geotek Limited
Daventry, Northamptonshire, NN11 8PB, United Kingdom

ABSTRACT

Electrical trees are one of the main mechanisms of degradation in solid polymeric insulation leading to the failure of high voltage equipment. They are interconnected networks of hollow tubules typically characterized from two-dimensional (2D) projections of their physical manifestation. It is shown that complete characterization requires a three-dimensional (3D) imaging technique such as X-ray computed tomography (XCT). We present a comprehensive set of parameters, quantitatively characterizing two types of tree topology, conventionally known as bush- and branch-type. Fractal dimensions are determined from 3D models and from 2D projections, and a simple quantitative relationship is established between the two for all but dense bush trees. Parameters such as number of nodes, segment length, tortuosity and branch angle are determined from tree skeletons. The parameters most strongly indicative of the differences in the structure are the number of branches, individual channel size, channel tortuosity, nodes per unit length and fractal dimension. Studying two stages of a bush tree's development showed that channels grew in width, while macroscopic parameters such as the fractal dimension and tortuosity were unchanged. These parameters provide a basis for tree growth models, and can shed light on growth mechanisms.

Index Terms — **electrical trees, three-dimensional trees, 3D imaging, fractal analysis, XCT**

1 INTRODUCTION

ELECTRICAL trees are a form of degradation in polymers exposed to high electric fields [1]. Despite extensive research, the fundamental mechanisms of initiation and tree growth are not fully understood. It is clear however, that the growth of electrical trees can lead to irreversible insulation failure. In power systems this results in a high-energy discharge accompanied by significant damage. A better understanding of this aging mechanism is key to development of new insulation designs, and to enabling asset management through condition monitoring.

The visible aspect of electrical trees is associated with hollow 1-10 μm diameter interconnected bifurcated tubes and resembles botanical trees. Their development is associated with partial discharges (PDs) and, in the laboratory, with high divergent fields typically generated using a needle electrode.

A variety of techniques has been used to image electrical trees [2]. The most common methods are optical imaging and scanning electron microscopy (SEM). Optical methods provide 2-dimensional (2D) images from transparent or translucent materials. SEM provides cross-sections of small parts of a tree. Conventional optical imaging uses a camera which presents a projection of the tree from one direction, perpendicular to its general direction of growth (typically extending from the axis of a needle electrode). Depending upon the depth of field only part of the tree (a slice) is captured in the projected image.

Key to the nature of an electrical tree (and its name) is its shape. Quantifying tree-type structures can be traced to Leonardo da Vinci, who introduced the notion of a fixed total thickness for a botanical tree as bifurcation points are passed, and who

Manuscript received on 4 April 2018, in final form 2 October 2018, accepted 8 October 2018. Corresponding author: R. Schurch.

DOI: 10.1109/TDEI.2018.007486

considered the angles of bifurcation [3]. Commonly, the shape of an electrical tree is categorized into branch, bush or bush-branch types [1]. Other distinctive shapes include branch-pine, bine-branch and monkey-puzzle [4-6].

Tree length (L) is commonly used to characterize a tree [4–7]. It is normally defined as the Euclidean distance from the needle tip to the furthest tree tip in a 2D projected image (see Figure 1a). Tree length analysis relates to remaining insulation life expectancy because the final breakdown process is expected to ensue rapidly once a tree crosses the insulation thickness. The tree growth rate (dL/dt) is often presented [4, 6, 8]. Another widely quoted property is fractal dimension (D_f) [4, 5, 8] which quantifies how a tree fills the space it occupies. D_f is typically calculated through the box-counting method, in which a 2D space is divided into squares (or cubes in 3D) with edge length r, and the number of squares required to cover the shape $N_{(r)}$ is counted. If $N_{(r)} \propto r^{-D_f}$ is satisfied, then D_f is the fractal dimension [9].

Three other quantities used to characterize electrical trees are: Firstly, the 'expansion coefficient' [5], which is defined as the ratio between the width (D) and the length of the tree (L), as defined in Figure 1a. Second, the accumulated damage [8], is the area covered by the tree structure in the projected image. Third, the relationship between number of branches and branch orders as deployed by Kudo [10].

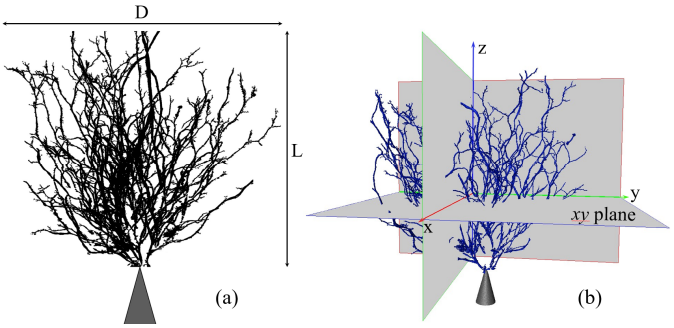

Figure 1. (a) Tree structure magnitudes in 2D images: length (L) and width (D), (b) Definition of the coordinate system of a 3D tree [12].

Analysis of tree growth using these parameters is limited because they are from 2D projected images. For example, the lengths determined from 2D projections are not the true branch lengths, and depend on the observation angle of the projection. Moreover, as pointed out by Kudo [9], the fractal dimension of 2D projections is not the same as the 3D value.

Recently, the authors have developed new methods of imaging electrical trees using serial block-face SEM (SBFSEM) and X-ray computed tomography (XCT) [2], [11]. This paper presents new methods of characterization and illustrates the deeper insight that 3D analysis can provide.

2 METHODOLOGY

The procedure for 3D imaging and analysis of electrical trees comprised the following: sample preparation, electrical tree creation, image acquisition, image segmentation and quantitative analysis [2, 11, 12]. The samples were cubes of 25 mm edge, prepared using a conventional needle-to-plane geometry with a gap of 2 mm between the needle tip (high voltage electrode) and the bottom of the sample (grounded). Two epoxy systems were studied: Araldite® LY5052-Aradur® HY5052, (glass transition temperature, T_g, of 120-130ºC), and Araldite® CY221-Aradur® HY2966 (T_g of 25-29ºC). An additional sample was made of a transparent photopolymer (Norland® Optical Adhesive 61). A summary of the samples is given in Table 1. In the first stage of this work, acupuncture needles (Hwato® 0.35 mm, ~5 µm tip radius) were used as the HV electrode. After realizing the importance of a highly symmetric needle tip for 3D imaging, Ogura needles of 1 mm diameter and 3 µm tip radius were used. Details of sample preparation are given in [12].

Table 1. Description of samples and electrical tests.

Sample	Material	Needle	Electrical stress		Length
			Voltage (kV)	Duration	(Optical)
1	LY5052/HY5052	Acup. ~5 µm	10	few sec.	< 0.1 mm
2	NOA 61	Acup. ~5 µm	8.5	3 h	~ 1.2 mm
3	CY221/HY2966	Ogura 3 µm	10-12	40 min	~ 0.1 mm
4		Ogura 3 µm	10-11	35 min	~ 1.1 mm
5		Ogura 3 µm	10	35 min	~ 0.7 mm
6		Ogura 3 µm	10	50 min	~ 1 mm
7		Ogura 3 µm	8	1h 55min	~ 1.2 mm
8		Ogura 3 µm	10	1h 55min	~ 1.2 mm
9		Ogura 3 µm	12	1h 55min	~ 1.4 mm

Trees were grown in each sample by applying a 50 Hz AC voltage of between 8 and 12 kV until the desired tree length was reached. Tree growth was monitored by an optical camera and by measuring PD activity. The magnitude of the RMS voltage and the duration of the test are shown in Table 1. Sample 5 was selected for a two-stage tree-growth experiment, detailed in Section 4.5. After tree growth, samples were machined to create a 2-3 mm diameter cylinder of polymer containing the tree to be imaged. Images of trees were obtained using XCT and SBFSEM. In this work we analyze only the datasets from XCT experiments but the techniques are equally applicable to SBFSEM data. A variety of XCT technologies were deployed [12]: micro or nano-XCT, and laboratory or synchrotron XCT. The lab systems are in Manchester and the synchrotron-based experiments were conducted at the Paul Scherrer Institut. A summary of the scan settings for image acquisition is presented in Table 2.

Table 2. Settings used for XCT scans.

Sample	Instru-ment	Distan. (mm)		Obj.	Energy (kV-keV)	Exp. Time (s)	# Proj.	Scan time (h:m)	Voxel size (µm)	# slices used
		S-S	S-D							
1	Lab.	30	25	20X	80	50	1501	22:27	0.371	160
2	Lab.	30	15	20X	80	60	1301	23:18	0.4535	1589
3	Lab.	11	5	40X	60	15	2001	9:46	0.2322	461
4	Syn.	N/A	21	10X	16	0.045	6001	0:05	0.65	1694
5	Lab.	17	8	20X	80	20	1301	8:19	0.4509	1434
6	Syn.	N/A	21	10X	16	0.045	6001	0:05	0.65	1328
7	Syn.	N/A	21	10X	16	0.045	6001	0:05	0.65	1833
8	Syn.	N/A	21	10X	16	0.045	6001	0:05	0.65	1914
9	Syn.	N/A	21	10X	16	0.045	6001	0:05	0.65	2096

Distances: S-S: Source-Sample. S-D: Source-Detector
Energy: Synchrotron: keV. Laboratory: kV.

In 3D imaging, the dataset comprises a stack of images (cross-sectional slices) obtained after the reconstruction process from the XCT scans. The image segmentation process uses the grey-scale levels of the slices, to identify and extract the electrical tree. The result is a new stack of images, where pixels are no longer grey-scale levels but color-labelled, each color representing a different material. In the case of electrical trees in unfilled epoxy, images are composed of only two colors: representing void (air) and epoxy resin. Segmentation was carried out using Avizo image processing software. More detail is given in [12]. This process yields 3D models (virtual replicas), as shown in Figure 2, for visualization and further quantification, as presented in the following section.

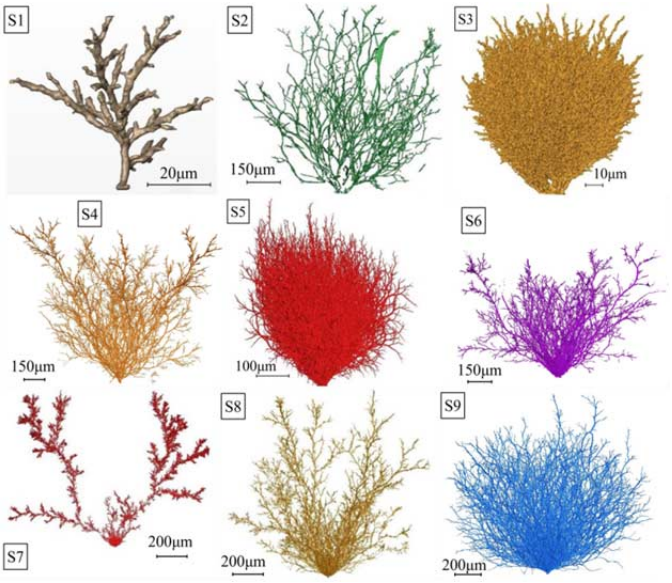

Figure 2. Virtual replicas of the samples.

3 CHARACTERIZATION METHODS FOR 3D ELECTRICAL TREES

3D visualization of complex structures provides great benefit by removing obfuscation of interior features. Moreover, it provides a 3D model (virtual replica) that can be fully categorized. Here features are classified as either global (associated with the macro tree), local (cross-sectional analysis of features), or parameters derived from the skeleton (center-lines) of the tree [12, 13]. To exemplify the calculation of the parameters, Sample 1 will be used throughout the following. A summary of the values obtained for all the samples is presented in Table 3. Analysis and interpretation of the parameters is provided in Section 4.

3.1 GLOBAL PARAMETERS

Global parameters are the indices calculated considering the entire structure of the tree: length, distribution of channel diameters, surface area, volume and convex hull volume.

Tree length was calculated by multiplying the number of slices in the virtual replica by the pixel size (the slice separation). This is the length of the tree in the needle axial direction. The diameters of tree channels are calculated using the method described in [14]. This involves determining the diameter of the largest sphere which contains the voxel under consideration and which is completely inside the structure. The result is a list with values representing the diameter of the sphere in which the voxel is contained, for all the voxels in the tree. Thus, the mean thickness corresponds to a volume-weighted distribution. Analysis of the diameter of tree channels is provided in Section 4.1.

The surface of the electrical tree is generated by computing a triangular approximation of the interface between the tree and the epoxy using Avizo software. The surface area, tree volume, and convex hull volume were also determined in Avizo. Tree volume is determined by multiplying the number of voxels labelled as 'electrical tree' by the voxel volume. The convex hull is the smallest convex polyhedral surface that contains the entire feature [2]. The convex hull is mainly used to calculate the proportion of volume occupied by the tree. Surface-to-volume and volume-to-length ratios were also determined.

The fractal dimension of the tree was estimated using the box-counting method (available in Matlab). The '3D fractal dimension' denoted $^{3D}D_f$ is the box-counting fractal dimension using 3D data, and $^{2D}D_f$ is the box-counting fractal dimension estimated from 2D projected patterns [15]. 2D patterns were obtained by projecting the 3D virtual replica (as in Figure 2) onto one of the orthogonal planes (*xz, yz*) (Figure 1b). This is equivalent to experimental optical images. The $^{2D}D_f$ value generated corresponds to the average of $^{2D}D_f$ from projections of *xz* and *yz* planes, since they were similar for all the samples. The analysis of fractal dimensions is presented in Section 4.2.

3.2 LOCAL PARAMETERS

Local parameters were developed by considering cross-sections in the *xy* plane, to investigate the change in the tree structure along its axial direction. These are defined as 'local' because they belong to a specific slice and not to the entire tree. For each slice the number, area and 2D convex hull area of tree channels were determined. From these, the proportion of area degraded, defined as the ratio of the sum of the channels' areas to the convex hull area, was calculated. The progression of these parameters along the axial direction of the tree is shown in the graphs of Figure 3. Analysis of these parameters is presented in Section 4.3.

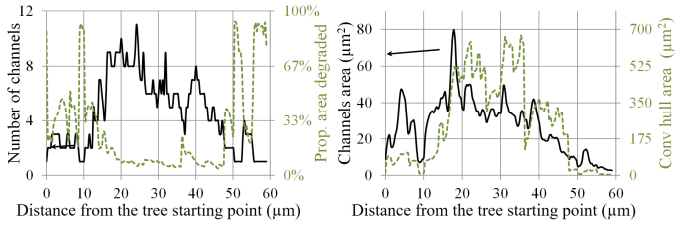

Figure 3. Progression of the number of tree channels and the proportion of area degraded in every cross-sectional slice as a function of the tree initiation point – Sample 1.

3.3 PARAMETERS FROM THE TREE SKELETON

Interconnected structures can be analyzed as networks by generating a 'skeleton', consisting of line segments following the centers of the channels connected at branch points (nodes). Thus, a segment (i.e. a branch) is the path between two nodes, and a node can be: an initiation point, a branching (bifurcation or merging) point, or an end point (tree tip). The skeleton was generated in Avizo software and is displayed in the form of a spatial graph as shown in Figure 4a. The number of nodes and segments are counted, and the end-point fraction, the proportion of nodes which are end points of the channels rather than branch points, is calculated.

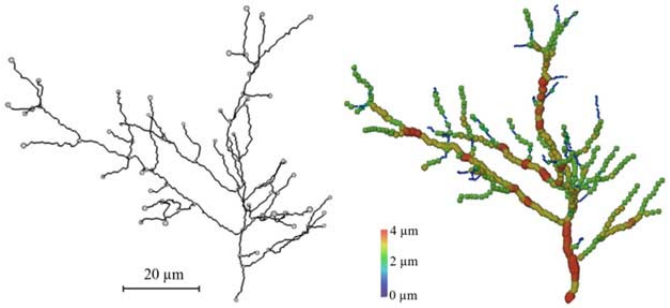

Figure 4. (a) Skeleton of the tree in Sample 1: interconnected network of segments and nodes. (b) Sphere-tree of Sample 1: composed of spheres with colors representing local channel diameter.

Node degree, segment length, tortuosity and branch angle are presented in the form of frequency distributions and the mean value and standard deviation determined. The node degree is the number of segments connected to each node (the branch order must be ≥3 in order for the node to be a branch point). The segment length is the distance between nodes, following the tree path. Tortuosity is a measure of the 'straightness' of the branches of the tree, calculated as the ratio between the length along the shortest route and the Euclidean distance from the initiation point to the end point of the branch. Shortest paths were determined using Dijkstra's algorithm [16]. The branch angle is the angle between line segments at a branch point. The branch angle was derived by first specifying a 'parent' line segment for a given node, this being the line segment that is reached first when traversing the tree from the initiation point of the tree. The vector angle between the beginning sections of the parent and each child line-segment was then calculated.

Other useful quantities can be calculated from the skeleton, such as node density and segment length-to-diameter ratio. Node density is the ratio between the number of nodes and the volume of the tree. The segment length-to-diameter is the mean segment length divided by the mean diameter of tree branches. The values obtained are presented in Table 3.

4 ANALYSIS

A variety of trees has been imaged with a range of instruments, allowing the impact of the imaging techniques on quantitative parameters to be determined [11].

4.1 THE DIAMETER OF TREE CHANNELS

The distribution of diameters of tree channels in Sample 1 is shown in Figure 4b, where the tree is modelled by colored spheres that represent the local diameter. The mean diameter provides a parameter for characterizing electrical trees. However, a single value cannot capture the complexity of the distribution of diameters, as shown in Figure 5. The histograms were generated from a random sample of 5,000 points of the entire list of diameters. The values for mean diameter and standard deviations in Table 3 were calculated using the entire set of data. Some bush-type samples had larger local diameters calculated than are shown on the

Table 3. Global parameters and parameters from the skeleton of the trees.

	Sample	1	2	3	4	5	6	7	8	9
Global parameters	Pixel size (xy / z) (µm)	0.371	0.4535	0.2322	0.65	0.4509	0.65	0.65	0.65	0.65
	Slices used	160	1,589	461	1,695	1,434	1,328	1,833	1,914	2,099
	Length (µm)	59	720	107	1,102	647	863	1,191	1,244	1,364
	Diameter (µm)	2.0 (18%)	3.1 (38%)	1.2 (28%)	2.7 (43%)	2.5 (25%)	3.1 (38%)	2.1 (21%)	2.4 (43%)	3.0 (43%)
	Surface area (μm^2)	3.50×10^3	7.67×10^5	2.49×10^5	2.07×10^6	2.60×10^6	1.71×10^6	1.29×10^6	2.54×10^6	7.11×10^6
	Volume (μm^3)	1.62×10^3	6.53×10^5	6.72×10^4	1.46×10^6	1.59×10^6	1.10×10^6	6.44×10^5	1.55×10^6	6.52×10^6
	Conv. hull volume (μm^3)	5.62×10^4	2.25×10^8	5.68×10^5	7.93×10^8	1.03×10^8	4.34×10^8	6.10×10^8	8.40×10^8	1.70×10^9
	Surface/Volume (μm^{-1})	2.16	1.18	3.70	1.42	1.64	1.55	2.00	1.64	1.14
	Volume/length (μm^2)	27	907	628	1,326	2,453	1,277	541	1,245	4,588
	Prop. volume degraded	2.9%	0.3%	11.8%	0.2%	1.5%	0.3%	0.1%	0.2%	0.4%
Fract. dim.	$^{3D}D_f$	1.69	1.94	2.33	1.86	2.16	1.89	1.78	1.89	1.99
	$^{2D}D_f$ - Average	1.46	1.75	1.76	1.66	1.79	1.69	1.63	1.69	1.76
Skeleton	Number of nodes	78	6,768	28,967	16,609	23,028	17,511	31,626	30,685	37,044
	Number of segments	78	6,908	38,792	12,739	29,431	17,499	38,723	32,063	32,072
	End point fraction	0.5	0.4	0.1	0.7	0.3	0.5	0.3	0.5	0.6
	Node degree	3.2 (12%)	3.1 (9%)	3.4 (22%)	3.0 (8%)	3.1 (10%)	3.3 (21%)	3.4 (26%)	3.4 (27%)	3.1 (9%)
	Segment length (µm)	7.3 (60%)	11.7 (118%)	2.3 (63%)	25.5 (107%)	12.7 (86%)	17.6 (118%)	10.6 (68%)	15.5 (102%)	32.9 (114%)
	Tortuosity	1.2 (6%)	2.5 (38%)	1.5 (6%)	1.3 (7%)	1.5 (12%)	1.4 (19%)	1.5 (16%)	1.5 (28%)	
	Branch angle (deg)	69 (39%)	63 (49%)	69 (46%)	64 (47%)	60 (45%)	69 (46%)	70 (45%)	71 (46%)	64 (47%)
	Node density (μm^{-3})	4.8×10^{-2}	1.0×10^{-2}	4.3×10^{-1}	1.1×10^{-2}	1.5×10^{-2}	1.6×10^{-2}	4.9×10^{-2}	2.0×10^{-2}	5.9×10^{-3}
	Seg. length/diameter	3.7	3.8	1.9	9.4	5.0	5.7	4.8	6.1	10.7

histogram because in those samples the region near to the needle tip was highly degraded resulting in large regions of damage. This destroyed the original tree structure and it is therefore inappropriate to determine the diameter of tree channels in that region as it is effectively a degraded volume rather than a network of channels. This degraded volume presents a significant void of 50-100 µm diameter in which PD may occur [17]. It is noted that the smallest diameter measured relates to the spatial resolution of the imaging system, and does not necessarily correspond to the smallest feature in the real tree. This issue is discussed in Section 5.1.

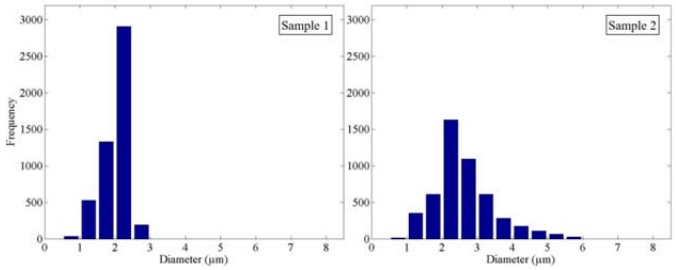

Figure 5. Histogram of diameter of tree channels for Samples 1 and 2.

4.2 FRACTAL DIMENSION

This section evaluates the error incurred when the fractal dimension is estimated from 2D projected images of the tree, rather than the 3D model. The authors have also reported previously that the method of determining the fractal dimension through box-counting affects the values of fractal dimension obtained [15]. However, the fractal dimension from 2D projections was not affected greatly by the angle of observation (counter to the finding in [18]). Values determined from the *xz* and *yz* projections are found to be within 5%. This is expected in a broadly rotationally symmetric structure, which is the case here.

The difference between the fractal dimension determined from the 2D projected patterns and from the 3D model is larger for dense bush trees such as Samples 3 and 5 (24% and 17% respectively); this is due to the loss of superimposed information in the projection. To correct the fractal dimension determined from 2D images, complex expressions to relate the true fractal dimension of the 3D structures and their projected 2D patterns have been proposed [9], [18]. Here we find that for dense bush trees for which ${}^{3D}D_f > 2$, 2D projections do not represent the complexity adequately and cannot be relied upon. However for ${}^{3D}D_f < 2$, the simple formula

$$ {}^{3D}D_f = {}^{2D}D_f + 0.2 \quad \text{if } {}^{2D}D_f < 1.75 \qquad (1) $$

represents the data well. Figure 6 illustrates the fit of equation (1), and that proposed by Kudo [8]. We find that for ${}^{3D}D_f > 2$ there is no quantitative equivalence to the D_f values because of the lost information from superimposed features.

4.3 LOCAL PARAMETERS

Local parameters can be used to investigate the change in structure as the tree grows, as shown in Table 4. This data was extracted from graphs such as Figure 3. Comparing the values

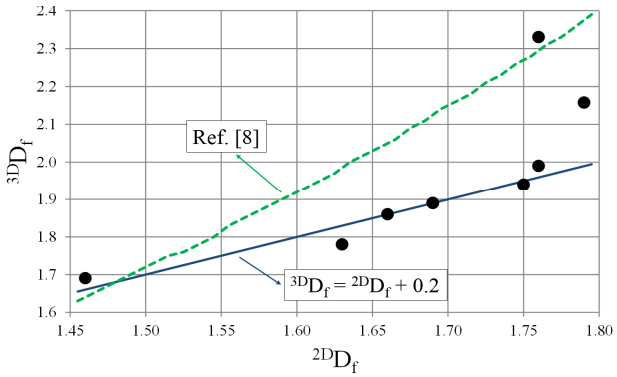

Figure 6. Relation of fractal dimension from 2D and 3D images. The solid line of best fit does not consider the points for which ${}^{3D}D_f > 2$. The dotted line is the equation proposed by Kudo [8].

Table 4. Summary of local parameters (in cross-sections orthogonal to the needle direction).

Sample	Length (µm)	Number of channels		Channel area (µm²)		Eq. channel area (µm²)		Proportion area degraded	
		Avg	Max	Avg	Max	Avg	Max	Avg	Max
1	59	5	11	27	80	7	24	27%	94%
2	720	58	115	906	1,714	16	51	1%	19%
3	107	202	446	628	1,328	4	48	19%	91%
4	1,102	99	209	1,326	2,977	14	150	3%	100%
5	647	306	684	2,453	5,867	11	293	5%	94%
6	863	112	302	1,277	3,870	11	42	2%	100%
7	1,191	56	141	541	1,519	9	33	3%	100%
8	1,244	110	438	1,245	4,051	12	106	3%	95%
9	1,364	227	491	4,581	11,254	18	69	1%	91%

gives information about the tree structure. It can be inferred, for example, that Sample 5 is a bush tree and conversely, Sample 1 a branch type. Bush and branch trees are more extensively compared in the next section.

Local parameters can be measured at the same distance from the tree starting point for all the samples, and thus provide a common comparison point [13]. Table 5 presents the local parameters measured at a distance of 40 µm from the tree initiation point including the volume of the tree up to that distance. This distance is large enough to avoid the massively degraded un-treelike region near the needle tip but small enough so that comparison can be made for all trees. The method of comparing trees at a fixed comparative point or plane is more representative than some global parameters. Bush-type trees such as in Samples 3, 5 and 9 gave considerably higher accumulated degraded volumes than branch trees (e.g. Sample 1). The total channel area in the slice 40 µm from the needle had an appreciably higher number of tree channels and associated net area in the cases of bush trees.

Table 5. Local parameters measured on a slice 40 µm distant from the tree initiation point.

Sample	1	2	3	4	5	6	7	8	9
Number of channels	7	15	346	21	80	197	124	214	66
Channels area (µm²)	32	630	1,242	560	1,839	2,478	695	2,433	1,548
Conv. hull area (µm²)	343	17,751	5,461	3,253	18,129	13,282	7,819	38,843	255,412
Prop. area degraded	9%	4%	23%	17%	10%	19%	9%	6%	1%
Acc. deg. volume (µm³)	1,396	9,772	23,866	8,735	40,887	41,495	18,433	38,421	15,502

4.4 BUSH AND BRANCH TREE TYPES

A basic differentiation between a bush and a branch tree is the number of branches. From cross-sectional analysis, the average number of tree channels per slice was over 100 in the cases of bush trees (e.g. Samples 3, 5 and 9) but less than 60 for branch trees (e.g. Samples 1 and 7). As expected [17], there was also a difference in channel size: bush trees had a mean diameter in the range 3-4 μm, whereas for branch trees this was around 2 μm. This is considered to be due to PD in a non-conducting bush tree being located in the main channels and body of the tree [7,17], causing widening of the channels; while in a conducting branch-tree the PDs are mainly in the tree tips, removing that mechanism of channel diameter increase. This parameter showed more variation than the fractal dimension. In most of the cases, the fractal dimension of bush and branch trees was higher than 2 and lower than 2 respectively, in accordance with the conventional classification [1].

Another parameter that is discriminative between bush and branch trees is the number of channels as a function of distance along the tree length, depicted in Figure 7a. Close to the tree origin, the rate of change is higher for bush trees than for branch trees. For bush trees the values were, for Samples 3, 5 and 9: 10.3, 4.0 and 2.7 channels/μm respectively; in contrast, branch trees had values below unity, e.g. Sample 1 develops at 0.8 channels/μm.

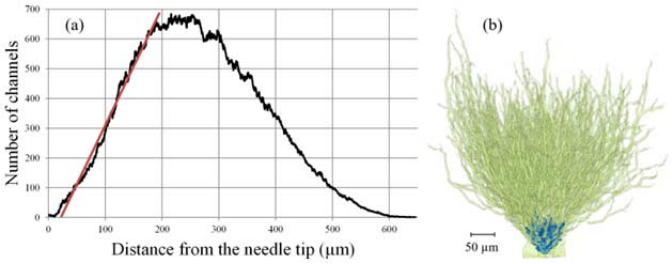

Figure 7. (a) Rate of increment of the number of tree channels, obtained from the slope of the linear regression (Sample 5). (b) Virtual replicas of Sample 5: first (blue) and second (green) stages of growth superimposed.

Another characteristic of bush trees is that the branches bifurcate more, thus the number of nodes per unit length can be used to distinguish between bush and branch trees. Branch trees had fewer than 5 nodes per μm, whereas bush trees had more than 10 nodes per μm. The end-point fraction index was also found to be discriminative. The end-point fraction for bush-type trees was generally smaller than for branch-type trees. Increased branching leads to tortuosity in branch trees of between 1.2 and 1.5, and in bush trees between 1.5 and 2.5.

4.5 ANALYSIS OF TWO STAGES OF GROWTH

Sample 5 was used for a two-stage tree-growth experiment. For the first stage, the sample was electrically stressed for 5 minutes and then XCT imaged. In the second stage, the sample was stressed for a further 30 minutes and imaged again. The same scan parameters were used in each stage for consistency in the comparison. It should be noted that although Sample 5 referred to in previous sections is the same specimen as the second stage presented here, the datasets are not the same, since this specimen was scanned a third time with different scan settings for improved results. The improved imaging results from the third scan were used for quantitative analysis. Details of the two-stage experiment can be found in [12], while the virtual replicas of both stages are shown superimposed in Figure 7b.

After the first stage a dense bush tree grew. The second stage of growth developed the bush tree further. The volume adjacent to the needle tip, which contained the tree after the first period, suffered a considerable increment in damage during the second period, resulting in a space with no distinguishable channels but an unstructured degraded volume instead. This degraded volume developed around, and even below the needle tip.

The progression of the number of tree channels as a function of the distance from the needle tip is plotted in Figure 8a. The results quantify that after the first period of aging the tree contained more channels in the region 0-40 μm from the needle tip than after the second stage, however the area covered by the channels in the second stage was greater. This was due to widening of the tubes that eventually merged, increasing the area but decreasing the number of channels. The overall shape of the curves obtained for the first and second stages was similar. The key features of the bush tree, including $^{3D}D_f$ and tortuosity, remained unchanged despite the volumes of the stages being very different.

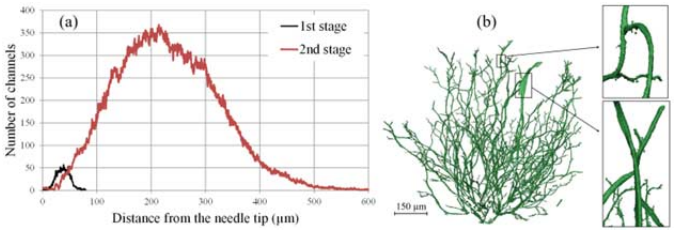

Figure 8. (a) Number of channels as a function of the distance from the needle tip for the first and second stages of Sample 5. (b) Sample 2 with magnifications showing merged branches.

A selection of tree characteristics of the first and second stage is presented in Table 6. As expected in a bush tree, the tree channels widened, increasing in mean diameter from 2.6 μm after the first stage to 3.7 μm after the second. Although the duration of the stress of the second stage was only 6 times the duration of the first (30 min and 5 min), the volume of the second stage was 78 times greater than that of the first. The longer mean segment length of the second stage (8.8 μm compared to 5.1 μm) suggests that branches of a more mature bush tree grow further before they bifurcate. This is in accordance with the greater node density measured for the first stage (0.037 vs. 0.011 μm^{-3}), revealing that more branching occurred in the first stage of growth. The fractal dimension of the tree and the tortuosity of the branches remained almost the same. A similar situation was reported in [4], in which bush trees were created in XLPE.

Table 6. Electrical tree characteristics of the first and second stage of growth in Sample 5.

	1st stage	2nd stage
Length (μm)	80	605
Mean channel diameter (μm)	2.6	3.7
Volume (μm^3)	2.50×10^4	1.95×10^6
Volume/length (μm^2)	313	3,227
${}^{3D}D_f$ Fractal Dimension	2.12	2.18
Number of nodes	927	21,121
Mean Segment length (μm)	5.1	8.8
Mean Tortuosity	1.6	1.6
Node density (μm^{-3})	3.7×10^{-2}	1.1×10^{-2}

5 DISCUSSION

5.1 3D STRUCTURAL CHARACTERISTICS

The accuracy and meaningfulness of the indices determined depend on how close the virtual replica is to the original tree geometry. In XCT, image segmentation is greatly affected by the image quality of the slices that were acquired in the scans. Moreover, the strategy and methods used for image segmentation influence the resulting virtual replica, and therefore, the quantitative parameters. Another point to consider is that the characterization tool presented here can only quantify what has been identified by the XCT scan. It is likely that fine details existed smaller than the spatial resolution of the resulting dataset, and so were missed and not considered in the characterization.

Comparisons between bush and branch trees are summarized in Table 7. Two key differences between the bush and branch trees are the density of channels and the frequency of branching, which are efficiently characterized by the volume-length ratio, the rate of increment of tree channels and the number of nodes per unit length.

Table 7. Comparison of parameters for bush and branch trees.

	Relative comparison	Bush tree	Branch tree
Channel diameter	Wider in bush trees	3-4 μm	~2 μm
Tree volume-to-length ratio	Higher in bush trees	> 1000 μm^2	< 500 μm^2
Number of channels /branches *	Higher in bush trees	> 100	< 60
Channel cross-sectional area *	Larger in bush trees	> 10 μm^2	< 7 μm^2
3D Fractal dimension	Higher in bush trees	> 2	< 2
Rate of growth of change of number of channels close to the origin	Higher in bush trees	> 3 μm^{-1}	< 1 μm^{-1}
Nodes per unit length	Higher in bush trees	> 10 nodes per μm	< 5 nodes per μm
Tortuosity	Higher in bush trees	1.5 – 2.5	1.2 – 1.5
Branch angle	Similar in both types	60º-70º	65º-70º

* Average per cross-section along a tree

The structure of electrical trees revealed in 3D contains information about the growth process in addition to the quantified characteristics. For example, Figure 8b shows merged branches in Sample 2. This observation suggests that this is a non-conducting structure. Tree growth is a field-driven process, and it is unlikely that in a conducting structure, channels, which would be at the same potential, would grow together. This phenomenon could not have been confirmed using conventional 2D imaging, because there would have been uncertainty over whether the two branches were close but in different planes, or were indeed merged.

5.2 INFORMING TREE MODELS

The quantification methods presented in this work provide a tool to evaluate assumptions for the formulation of tree propagation models [19-23]. Tree structures generated by computational-growth models do not presently provide the level of detail observed in the experimental tree replicas obtained in this work. This is mainly due to computational constraints. Most models impose a rectangular grid and with this, the growth path is limited to the nodes provided. This limits the degree of freedom and thus, simulated trees normally have a fixed segment length and only a few possibilities of branch angle. Nevertheless, structural parameters such as segment length, required in tree growth models, can now be validated (or contradicted). For example, the length of the new extended branch used in the discharge-avalanche model (DAM) [19] was 10 μm, which is in the range of the values measured here. Another key parameter is the branch angle. Most of the models for tree propagation use a rectangular grid. This allows branch angles of 0° or 90°. The model proposed in [20] allows branch angle values of 45°. Relatively more freedom of growth direction was provided by the model proposed by Noskov et al. [21]. The values obtained from the experiments presented here were in the range of 60-70° and did not show a significant difference between bush and branch trees.

Another consideration for the models that use the fractal dimension to simulate the growth is that the fractal dimension should be obtained from 3D tree structures and not from 2D projections. However equation (1) may be used if ${}^{2D}D_f < 1.75$, that is, if the tree is not too dense, otherwise 2D imaging is not adequate.

Widening of tree channels was observed in the two-stage tree-growth experiment (Section 4.5); however, neither the DAM nor the Noskov models considered this effect. In the DAM case a 1 μm radius was assumed [19], and Noskov used 5 μm radius spheres to create the tree structure. In contrast, Dodd [22] allowed widening of tree channels, with an initial radius of 1 μm for the newly-formed branch and a maximum radius of 25 μm (related to the grid spacing of 50 μm).

Many of the physical models proposed for tree propagation are based on the concept that the material damage (and consequently tree extension) originates from the energy dissipated by PDs within the tree. Using the tools developed in this work, the external electrical energy fed into the terminals of a sample during PD activity and the tree volume degraded was directly compared [24]. The vaporization energy, which is the energy required to dissociate the atoms from the material

previously within the tree channels, was found to be around 7% of the PD energy at the external terminals. This free parameter, that in physical models such as [22] controls the tree propagation rate, was previously estimated to be around 1-5% [25]. The updated value of 7% can be used in the physical models of tree growth to relate PD energy and material damage, and thus to control the simulated tree growth rate.

The bush tree characterized at two stages of tree-growth was imaged at lengths of 80 and 605 μm. The tree volume grew by a factor of 78 between images. Nonetheless, the key features of the tree remained unchanged, including fractal dimension and tortuosity. This indicates a consistency in mechanisms controlling the tree process. In this case, if it is assumed that the field at the tree tip is changing as the tree grows, we conclude growth is driven by partial discharge activity at the needle tip for the duration of the experiment.

6 CONCLUSIONS

A comprehensive tool for 3D analysis of electrical trees has been presented. Virtual replicas of electrical trees have been generated using XCT, from which conventional and new parameters were calculated and evaluated for structural discrimination. For a deep analysis of tree morphology, the 3D structure must be characterized with a set of parameters rather than only tree length or fractal dimension, as is common practice.

The structure of electrical trees has been characterized through global parameters (considering the entire tree), local parameters (considering cross-sections of the tree) and parameters derived from the skeleton of the tree. Global parameters including: volume, surface area, the proportion of volume degraded, and the distribution of the diameter of tree channels were determined. The mean diameter of tree channels was around 2 μm and 3-4 μm for branch and bush tree types, respectively. The degraded-volume to length ratio is discriminative: for bush trees the ratio was thousands of μm^2, while for branch trees it was in the range of tens to hundreds of μm^2. The fractal dimensions from both the 3D volume and the 2D projected patterns were calculated. The fractal dimension from 2D projections was not greatly affected by the angle of observation because the trees were mostly rotationally symmetrical structures. 2D characterization of fractal dimensions were not representative of 3D structure in dense bush trees. However, a linear relationship was found between 2D and true 3D values if ${}^{2D}D_f < 1.75$ and ${}^{3D}D_f < 2.0$, that is, if the tree is not too dense.

Local parameters from cross-sections at given locations along the tree were also calculated. Variation along the tree length was analyzed using the number of tree channels and the area covered by them. This methodology provided a powerful tool to quantify the internal structure of trees and compare different tree types. On average the number of branches 40 μm into a bush tree was greater than 100, compared to fewer than 60 for a branch tree. Close to the tree origin, the rate of change of the number of tree channels was over 3 channels/μm for bush trees and, in contrast, branch trees had values below 1.

Using the tree skeleton, parameters such as number of nodes, node density, segment length, tortuosity and branch angle were calculated. Overall, the parameters were indicative of differences in tree growth and can be used to classify the structure of electrical trees. The number of nodes per unit length of tree channel and the tortuosity have been shown to be discriminative. Characteristic values for bush and branch trees are respectively: >10 and <5 μm^{-1}; and 1.5-2.5 and 1.2-1.5. For the first time the branching angle has been fully characterized: angles were in the range of 60-70º irrespective of tree type.

One bush tree was characterized at two stages of tree-growth, with lengths of 80 and 605 μm. The key topological features of the tree remained unchanged whilst the volume grew by a factor of 78. It is concluded that, in this case, the prime mechanism for tree growth is unaltered during the treeing process.

ACKNOWLEDGMENT

The authors thank Universidad Técnica Federico Santa María for the grant PI_L_18_19, and Anne Bonnin at the Paul Scherrer Institut for her assistance in the XCT experiments in the award TOMCAT/SLS 20140325. This work was partially funded by the RCUK's Top & Tail Transformation project EP/I031707/1. RB would like to acknowledge funding from Carl Zeiss XRM, while at Manchester. This paper contains data openly available from www.manchestertrees.com

REFERENCES

[1] L. A. Dissado and J. C. Fothergill, *Electrical Degradation and Breakdown in Polymers*. London: Peter Peregrinus Ltd., 1992.

[2] R. Schurch, S. M. Rowland, R. S. Bradley, and P. J. Withers, "Imaging and analysis techniques for electrical trees using X-ray computed tomography," *I*EEE Trans. Dielectr. Electr. Insul., vol. 21, no. 1, pp. 53–63, 2014.

[3] J. P. Richter, *The notebooks of Leonardo da Vinci*. Revised ed., vol. 1. Dover, 1970, pp. 205-211.

[4] C. Xiangrong, X. Yang, C. Xiaolong, S. J. Dodd, and L. A. Dissado, "Effect of tree channel conductivity on electrical tree shape and breakdown in XLPE cable insulation samples," IEEE Trans. Dielectr. Electr. Insul., vol. 18, no. 3, pp. 847–860, 2011.

[5] Z. Xiaoquan and G. Chen, "Propagation mechanism of electrical tree in XLPE cable insulation by investigating a double electrical tree structure," IEEE Trans. Dielectr. Electr. Insul., vol. 15, no. 3, pp. 800–807, 2008.

[6] M. Bao, X. Yin, and J. He, "Structure characteristics of electrical treeing in XLPE insulation under high frequencies," Phys. B Condens. Matter, vol. 406, no. 14, pp. 2885–2890, 2011.

[7] C. Laurent and C. Mayoux, "Analysis of the Propagation of Electrical Treeing Using Optical and Electrical Methods," IEEE Trans. Electr. Insul., vol. EI-15, no. 1, pp. 33–42, 1980.

[8] G. Chen and C. Tham, "Electrical treeing characteristics in XLPE power cable insulation in frequency range between 20 and 500 Hz," IEEE Trans. Dielectr. Electr. Insul., vol. 16, no. 1, pp. 179–188, 2009.

[9] K. Kudo, "Fractal analysis of electrical trees," IEEE Trans. Dielectr. Electr. Insul., vol. 5, no. 5, pp. 713–727, 1998.

[10] K. Kudo, "On the regularity of the branching structure of electrical trees," Symp. Electr. Insul. Materials, 1988, pp. 203–206.

[11] R. Schurch, S. M. Rowland, R. S. Bradley, and P. J. Withers, "Comparison and Combination of Imaging Techniques for Three Dimensional Analysis of Electrical Trees," IEEE Trans. Dielectr. Electr. Insul., vol. 22, pp. 709–719, 2015.

[12] R. Schurch, "Three-Dimensional Imaging and Analysis of Electrical Trees," PhD Thesis, The University of Manchester, UK, 2014.

[13] R. Schurch, S. M. Rowland, R. S. Bradley, and P. J. Withers, "Three dimensional characterisation of electrical trees,"*Annu. Rep. Conf. Electrl Insul. Dielectr. Phenom. (CEIDP),* 2013, pp. 494–497.
[14] T. Hildebrand and P. Rüegsegger, "A new method for the model-independent assessment of thickness in three-dimensional images," J. Microsc., vol. 185, no. 1, pp. 67–75, 1997.
[15] R. Schurch, C. González, P. Aguirre, M. Zuniga, S. M. Rowland, and I. Iddrissu, "Calculating the fractal dimension from 3D images of electrical trees," IEEE *Int. Symp. High Voltage Eng. (ISH)*, 2017.
[16] E. W. Dijkstra, "A note on two problems in connexion with graphs," Numer. Math., vol. 1, no. 1, pp. 269–271, 1959.
[17] J. V Champion and S. J. Dodd, "Simulation of partial discharges in conducting and non-conducting electrical tree structures," J. Phys. D. Appl. Phys., vol. 34, no. 8, p. 1235, 2001.
[18] H. Uehara and K. Kudo, "The 3-D fractal analysis of electrical trees using a serial sectioning method and a CT method," *IEEE Int. Conf. Conduct. and Breakdown Solid Dielectr. (ICCBSD)*, 1998, pp. 309–312.
[19] L. A. Dissado and P. J. J. Sweeney, "Physical model for breakdown structures in solid dielectrics," Phys. Rev. B, vol. 48, no. 22, pp. 16261–16268, 1993.
[20] H. J. Wiesmann and H. R. Zeller, "A fractal model of dielectric breakdown and prebreakdown in solid dielectrics," *J. Appl. Phys.,* vol. 60, no. 5, pp. 1770–1773, 1986.
[21] M. D. Noskov, A. S. Malinovski, M. Sack, and A. J. Schwab, "Self-consistent modeling of electrical tree propagation and PD activity," IEEE Trans. Dielectr. Electr. Insul., vol. 7, no. 6, pp. 725–733, 2000.
[22] S. J. Dodd, "A deterministic model for the growth of non-conducting electrical tree structures," J. Phys. D. Appl. Phys., vol. 36, no. 2, pp. 129–141, 2003.
[23] G. E. Vardakis and M. G. Danikas, "Simulation of electrical tree propagation using cellular automata: The case of conducting particle included in a dielectric in point-plane electrode arrangement," J. Electrostat., vol. 63, no. 2, pp. 129–142, 2005.
[24] R. Schurch, S. M. Rowland, and R. S. Bradley, "Partial discharge energy and electrical tree volume degraded in epoxy resin," *Annu. Rep. Conf. Electr. Insul. Dielectr. Phenom. (CEIDP)*, 2015, pp. 820–823.
[25] M. A. Brown, J. V Champion, S. J. Dodd, and P. Mudge, "An investigation of partial discharge energy dissipation and electrical tree growth in an epoxy resin," *IEEE Int. Conf. Solid Dielectr. (ICSD)*, 2004, pp. 288–291.

Roger Schurch (S'11, M'15) received the degree in electrical engineering in 2006 from Federico Santa Maria Technical University (UTFSM). He was a high voltage equipment analyst at Transelec Transmission Company, before joining UTFSM, as Lecturer in 2008. He completed his PhD in 2014 at The University of Manchester and re-joined UTFSM as Assistant Professor. His research interests are electrical trees and partial discharges, and insulation diagnostics of power system plant.

Jorge Alfredo Ardila Rey received the M.Sc. and Ph.D. degrees in electrical engineering from Universidad Carlos III de Madrid in 2012 and 2014, respectively. He is currently working as a Professor at the Department of Electrical Engineering of UTFSM in Santiago, Chile.

Johny Montaña (M'00) is full time professor of the Department of Electrical Engineering at UTFSM, Chile. He received his Electrical Engineer degree in 1999, M.Sc. in High Voltage in 2002 and Ph.D. in Electrical Engineering in 2006 from Universidad Nacional de Colombia. His employment experiences include Siemens SA (2006-2009) and full time professor at Universidad del Norte, Colombia (2010-2013).

Alejandro Angulo (M'06) received the B.Sc. and M.Sc. degrees in electrical engineering from UTFSM, Valparaíso, Chile, in 2004 and 2007, respectively, and the Ph.D. degree in operational research from the Universidad de Chile, Santiago, Chile, in 2015. He is currently an Assistant Professor with the Department of Electrical Engineering, UTFSM.

Simon M. Rowland (F '14) graduated in physics from The University of East Anglia, and gained a PhD at London University. He worked in commercial research before joining The School of Electrical and Electronic Engineering in The University of Manchester in 2003. He was appointed Professor of Electrical Materials in 2009, and Head of School in 2015. He was President of the IEEE Dielectric and Electrical Insulation Society in 2011 and 12.

Ibrahim Iddrissu received his BEng in Electrical and Electronic Engineering at London South Bank University in 2011. He received his PhD in 2016 from the University of Manchester where he is currently a Research Associate.

Robert S. Bradley completed BA and MSc degrees in Natural Sciences (physics) at Cambridge University before gaining a Ph.D. in fluorescence imaging at The University of Manchester. He worked in the Henry Moseley X-ray Imaging Facility from 2008-2015, and in 2016 he joined Geotek Ltd, Daventry, UK, as Head of Development.